Microchemical Journal 141 (2018) 271–278

Contents lists available at ScienceDirect

Microchemical Journal

journal homepage: www.elsevier.com/locate/microc

Cysteine functionalized bio-nanomaterial for the affinity sensing of Pb(II) as an indicator of environmental damage

María L. Ramírez[a], Cecilia S. Tettamanti[a], Fabiana A. Gutierrez[a], Jose M. Gonzalez-Domínguez[b], Alejandro Ansón-Casaos[b], Javier Hernández-Ferrer[b], María T. Martínez[b], Gustavo A. Rivas[a,*], Marcela C. Rodríguez[a,*]

[a] INFIQC, Departamento de Físico Química, Facultad de Ciencias Químicas, Universidad Nacional de Córdoba, Ciudad Universitaria, 5000 Córdoba, Argentina
[b] Instituto de Carboquímica (CSIC), C/Miguel Luesma Castán 4, E-50018 Zaragoza, Spain

ARTICLE INFO

Keywords:
Single walled carbon nanotubes (SWCNT)
Cysteine functionalized bio-nanomaterial
Covalent functionalization
Affinity electrochemical biosensor
Lead affinity biosensing
Environmental damage

ABSTRACT

This work aims at the development of an electrochemical affinity biosensor for Pb(II) quantification using a platform that combines glassy carbon electrodes (GCE) and an aqueous dispersion of single-walled carbon nanotubes (SWCNT) covalently modified with cysteine residues (Cys). The biosensing protocol includes the accumulation of Pb(II) at the electrode surface through the affinity interaction promoted by Cys residues at open circuit potential, followed by the reduction of the accumulated Pb(II) at -0.900 V and the transduction step performed by linear sweep-adsorptive stripping voltammetry (LSAdSV) in a 0.020 M acetate buffer solution pH 5.00. There is a linear relationship between Pb(II) oxidation peak current and Pb(II) concentration. The dynamic linear range extends from 5.0 to 125.0 $\mu g \cdot L^{-1}$, exhibiting a sensitivity of 0.061 $\mu A \mu g^{-1} L$ and a detection limit of 0.69 $\mu g \cdot L^{-1}$. In addition, the selectivity of the biosensor was evaluated in the presence of high concentrations of possible interferents such as Cu(II), Cd(II), Ni(II), Hg(II), Rh(II), Ru(II), Zn(II), Ir(IV), Co(II) and As (III) demonstrating a high discrimination of Pb(II) in complex samples. The sensor was challenged with tap and rain water samples enriched with Pb(II), demonstrating outstanding properties in terms of recovery percentages showing an excellent agreement with ICP- MS.

1. Introduction

The increasing industrialization and urbanization over the past few decades led to the pollution of water due to the discharge of several toxic agents into ecosystem. This issue has become a major global concern [1]. Effluents may contain different kinds of toxic wastes like heavy metals and synthetic chemicals such as pesticides, pharmaceuticals, among other harmful contaminants [2,3]. It is widely known that the main sources of heavy metals are derived from industrial and agricultural activities like the use of pesticides and fertilizers, mining processes, fossil fuel, metallurgical and plastics production [3,4]. Heavy metals are non-biodegradable and ubiquitously spread, in addition, they are leading the ranking of harmful environmental chemicals since human and cattle health could be seriously damaged by long-term exposure and accumulation due to the ingestion of contaminated food and drinking water [3,5–7].

Lead, chromium, cadmium, mercury, nickel, copper and zinc are present at high levels in wastewater, mainly in undeveloped countries [8,9]. Among them, lead is a general metabolic poison and enzyme inhibitor which can be accumulated in bones, liver, brain, kidney and muscles [6,7]. Consequently, long term incorporation of lead can cause serious disorders like anemia, kidney disease, severe damage to the nervous system and mental retardation, especially children who are more likely to absorb and retain lead [5,7,10,11]. According to World Health Organization (WHO), the provisional guideline value for lead in drinking water is 0.010 mg L^{-1} [12]. These issues emphasize the importance of developing reliable, highly sensitive, user-friendly and cost effective tools for detection of heavy metals in different samples.

Considering the fact that detection and removal of these toxic ions is essential for the human well-being, several analytical techniques have been developed in order to survey drinking water, wastewaters and other samples that could be potentially in contact with them [13–15]. The most commonly used analytical techniques for their quantification include gas chromatography/mass spectrometry (GC/MS), inductively coupled plasma-mass (ICP-MS) and atomic absorption spectroscopy (AAS), among others [16–19]. Though highly sensitive, these analytical techniques are time-consuming, expensive, require experienced operator and are not easy to be employed in the field due to their bulky

* Corresponding authors.
E-mail addresses: grivas@fcq.unc.edu.ar (G.A. Rivas), marcela.rodriguez@fcq.unc.edu.ar (M.C. Rodríguez).

https://doi.org/10.1016/j.microc.2018.05.007
Received 26 January 2018; Received in revised form 24 April 2018; Accepted 7 May 2018
Available online 31 May 2018
0026-265X/

size. Overcoming these limitations, chemical sensors have emerged as an alternative for a simple, rapid, cost-effective and portable tool to analyze environmental security threats [15,20]. Among them, (bio) sensors are self-contained integrated devices that are capable of providing analytical information by integrating a biorecognition element which is in direct spatial contact with a transduction element [21,22]. In particular, electrochemical biosensors are simple to operate, facile fabrication and device integrated. These features make them outstanding alternative tools for a wide range of analytical purposes [15,20–23].

Advancements in the field of nanotechnology, especially the development of nano(bio)materials, have opened a new era for Analytical Chemistry [15,24]. Nanomaterials exhibit unique characteristics which contribute to its extensive applications in electrochemistry [25,26]. Among them, multi-walled carbon nanotubes (MWCNTs) and single walled carbon nanotubes (SWCNTs) have interesting physical, chemical and electrical properties that make them excellent candidates for the development of electrochemical biosensors [27–29]. However, due to the strong π-π interactions between their aromatic rings, CNTs tend to aggregate in aqueous solutions, making difficult their dispersion and further use for the development of electrochemical (bio)sensors [30–32]. Therefore, covalent or non-covalent functionalization of CNTs is a key alternative to avoid this problem [33]. The covalent functionalization of CNTs is more robust and better controllable as compared to non-covalent based methods [34–39]. Covalent functionalization also offers the possibility of establish a selective interaction and the ability to pre-concentrate a given analyte before its quantification. Amino acids have been reported as possible biorecognition molecules for the selective determination of heavy metals due to the presence of sulfur, nitrogen and/or oxygen atoms that can be recognized via the cooperative metal–ligand interaction [40–43]. In this sense, the use of glassy carbon electrodes (GCE) modified with poly-histidine have demonstrated to be very useful for the highly selective quantification of Cu(II) [44]. Recently, we reported the covalent functionalization of SWCNT with Cys and the development of a sensitive and selective biosensor for Cd (II) quantification as a model analyte [45].

This work proposes SWCNT-Cys dispersion as a suitable platform with unique properties for Pb(II) selective and sensitive quantification based on the high affinity of Cys residues towards Pb(II) [40]. SWCNT-Cys dispersion and the obtained biosensor (SWCNT-Cys/GCE) were critically studied. The optimal dispersion conditions as well as the correct transducer functionalization were investigated by electrochemical impedance spectroscopy zeta potential and linear adsorptive sweep voltammetry (LAdSV) measures. Experimental parameters, such as the deposition time and reduction time, were optimized by LAdSV. Finally, the electrochemical sensor was applied to the quantification of Pb(II) in real samples demonstrating outstanding capabilities in comparison with reference methods such as ICP-MS.

2. Experimental

2.1. Reagents

SWCNTs (AP-SWNT grade) were purchased from Carbon Solutions Inc., Riverside, California. The supporting electrolyte for the electrochemical assays was 0.020 molL^{-1} acetate buffer solution pH 5.00 (ABS), prepared by mixing stock standard solution of acetic acid and sodium acetate obtained from J.T. Baker. $Hg_2(NO_3)_2H_2O$ and As_2O_3 was obtained from Biopack; $Pb(CH_3COO)_2Pb(OH)_2$ and $(CdSO_4)_3.8H_2O$ were obtained from Anedra. Sodium dodecylbenzenesulfonate (SDBS), anhydrous *N,N′*-dimethylformamide(DMF), o-(benzotriazol-1-yl)-N,N,N´,N´-tetramethyluroniumhexafluorophosphate (HBTU), N,N-diisopropylethylamine (EDIPA), *S*-triphenylmethylcysteine (S-Trt-Cys), trifluoroacetic acid (TFA), $NiCl_2.6H_2O$, $Zn(NO_3).6H_2O$ were purchased from Sigma-Aldrich. Atomic absorption standard solutions of copper, rhodium, ruthenium, iridium were provided by Merck, while $CoSO_4.7H_2O$ was purchased from Dalton. Ultrapure water (p = 18.2MΩ cm) from a Millipore-MilliQ system was used for preparing all the solutions.

2.2. Apparatus

Electrochemical experiments were performed with an Autolab PGSTAT 128 N potentiostat (EcoChemie). Glassy carbon electrodes (GCE, CH Instruments, 3 mm diameter) were used as working electrodes. A platinum wire and Ag/AgCl, 3 M NaCl (BAS, Model RE-5B) served as counter and reference electrodes, respectively. All potentials are referred to the later. The electrodes were inserted into the conventional electrochemical cell through holes in its Teflon cover. A magnetic stirrer set at 800 rpm provided the convective transport during the pre-concentration step (previous to stripping experiments).

Electrochemical Impedance Spectroscopy (EIS) measurements were performed with an Autolab PGSTAT 128 N potentiostat (EcoChemie). The redox probe was 0.020 mol L^{-1} hydrogen peroxide prepared in a 0.050 mol L^{-1} phosphate buffer solution (PBS) pH 7.40 and the working potential was −0.100 V.

The zeta potential (Z) was determined by electrophoretic light scattering (ELS) measurements, using a Delsa Nano C instrument (Beckman Coulter).

Infrared spectroscopy (FTIR) measurements were performed with a Bruker Vertex 70 spectrometer. The samples were prepared with spectroscopic-grade KBr.

2.3. Cysteine-covalent functionalization of SWCNT (SWCNT-Cys) and preparation of SWCNT-Cys dispersion

The obtention of SWCNT covalently modified with Cys was published elsewhere [45]. Briefly, SWCNTs were purified in-house by air oxidation (350 °C, 2 h) followed by reflux in HCl (3 M, 2 h). Later, SWCNT were oxidized in a H_2SO_4/HNO_3 mixture (50:50 ratio, during 3 h), then they were dispersed in SDBS by ultracavitation and purged in an Ar atmosphere. The carboxylic activation was performed using HBTU/EDIPA for later interaction with L-S-Trityl-Cys dissolved in DMF. The deprotection of the thiol group was accomplished by using TFA and a silane derivative acting as scavenger. The final product was filtered, rinsed and dried under vacuum. Modified SWCNT were characterized by FTIR, TGA, XPS and Raman [45].

SWCNT-Cys dispersion was obtained by mixing 0.50 mg of covalently modified SWCNT-Cys with 1.0 mL of ultrapure water followed by 5 min of ultracavitation. Similar procedure was followed in order to prepare SWCNT and oxidized-SWCNT (SWCNT-Ox) dispersions for control experiments.

2.4. Preparation of SWCNT-Cys-modified GCE (SWCNT-Cys/GCE)

Prior to modification, GCEs were polished with alumina slurries of 1.0, 0.30 and 0.05 qm for 2 min each and then sonicated in ultrapure water for 10 s. The pretreated electrodes were dried with a stream of nitrogen. After that, GCEs were modified with SWCNT-Cys dispersion in the following way: an aliquot of 20 μL was dropped on top of each polished GCE and then the solvent was allowed to evaporate at room temperature.

2.5. Procedure

The capture of Pb(II) at SWCNT-Cys/GCE through complex formation was carried out at open circuit potential (OCP) for 7.0 min under stirring conditions. After the accumulation step, the electrode was thoroughly rinsed with 0.020 mol L^{-1} acetate buffer solution (ABS) pH 5.00 for 10 s and then transferred to a cell containing fresh 0.020 mol L^{-1} ABS pH 5.00. At this stage, the potential of the electrode was kept at −0.900 V for 3.0 min without stirring in order to reduce the

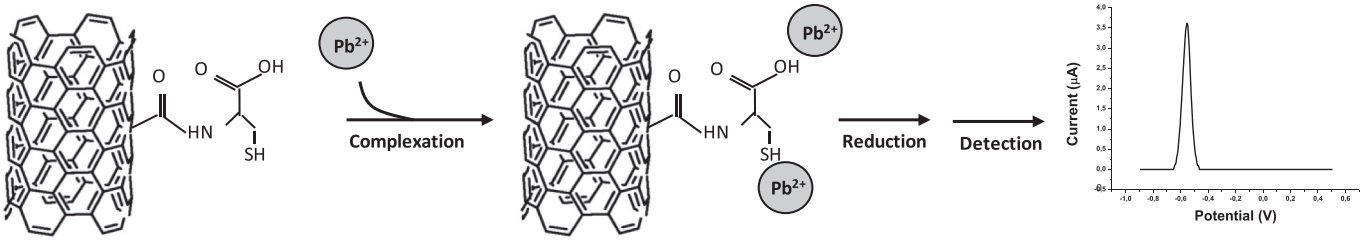

Scheme 1. Proposed recognition mechanism of Cys-functionalized SWCNTs (SWCNT-Cys) towards Pb.

captured metal and finally, the stripping was performed by LSAdSV between −0.900 V to 0.800 V with a step increment of 5.0 mV and scan rate of 0.150 Vs^{-1}.

The analytical signal was obtained using three electrodes for each experiment after subtracting the background current (Scheme 1). All the experiments were conducted at room temperature.

3. Results and discussion

3.1. Characterization of SWCNT-Cys dispersion

Fig. 1 shows SEM images for SWCNT-Ox/GCE (Fig. 1A) and SWCNT-Cys/GCE (Fig. 1B). The images show that carbon nanostructures completely cover the glassy carbon disk. However, in the case of SWCNT-Cys dispersion (Fig. 1B) the nanotubes are densely patterned and integrated, demonstrating an improved coverage of the glassy carbon surface. These results strongly suggest that the presence of Cys at the surface of SWCNT facilitates and promotes the dispersion of these modified SWCNTs and its homogeneous and robust deposition onto the glassy carbon surface.

The electrical properties of SWCNT-Cys/GCE surface were obtained from EIS experiments. Fig. 2 displays the Nyquist plots obtained at −0.100 V for SWCNT/GCE (A), SWCNT-Ox/GCE (B) and SWCNT-Cys/GCE (C) using a 0.020 M H_2O_2 solution as redox probe. The obtained experimental data were fitted with a Randles equivalent circuit (Fig. 2, inset), where R_s is the solution resistance, R_{ct} is the electron transfer resistance and Q_{dl} is a constant phase element modeling the double layer capacitance. The R_{ct} values obtained at the different electrodes were $(1.9 \pm 0.3) \times 10^4\,\Omega$, $(1.6 \pm 0.1) \times 10^4\,\Omega$ and $(1.3 \pm 0.1) \times 10^4\,\Omega$, for SWCNT/GCE (a), SWCNT-Ox/GCE (b) and SWCNT-Cys/GCE (c), respectively. From the analysis of the experimental R_{ct}, the increment of oxygenated groups in the nanostructure facilitates the electron transfer of the redox probe. As might be expected, Cys residues partially block the SWCNTs surface [45]. On the other hand, for this redox probe, the incorporation of a great number of Cys groups produces a decrease in the R_{ct} value, which is attributed to the catalytic activity of the Cys-thiol group towards H_2O_2 [46].

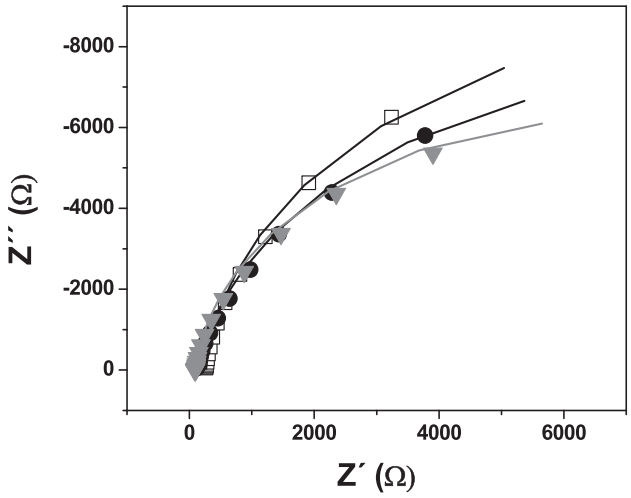

Fig. 2. Nyquist plot for the impedance spectra obtained for: SWCNT/GCE (A), SWCNT-Ox/GCE (B) and SWCNT-Cys/GCE (C). Frequency range: $1.0 \times 10^{-1} - 1.0 \times 10^5$ Hz, potential perturbation: 0.010 V, working electrode potential: −0.100 V, redox indicator: 0.020 $molL^{-1}$ H_2O_2 solution. Supporting electrolyte: saline buffer phosphate pH: 7,40.

The magnitude of the electrostatic charge properties of the platforms containing modified SWCNT can be determined by Z-potential measurements of the SWCNTs water dispersions. Z-potential assays at different pH values were performed for both modified dispersions SWCNT-Ox and SWCNT-Cys and the unmodified one (SWCNT) as a control (Fig. 1 SI). As it can be seen, the unmodified SWCNT present a low negative charge density in a wide pH range, due to the purification process, being the isoelectric point close to 4. SWCNT-Ox show a higher negative charge and changes in the surface properties as a consequence of the oxidation procedure in strong acidic media, due to the incorporation of different oxygenated groups, as can be observed by FTIR (Fig. 2 SI). The FTIR spectra shows that oxidation process introduces

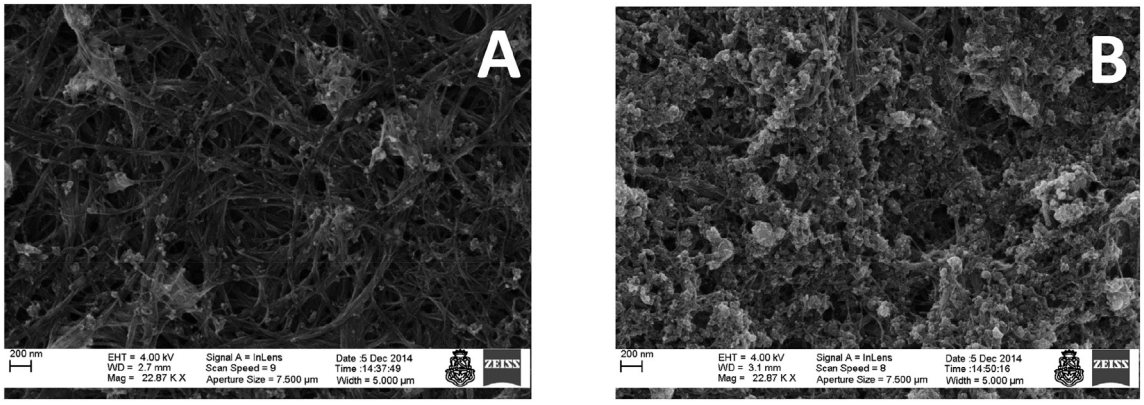

Fig. 1. SEM images for SWCNT-Ox/GCE (A) and SWCNT-Cys/GCE (B).

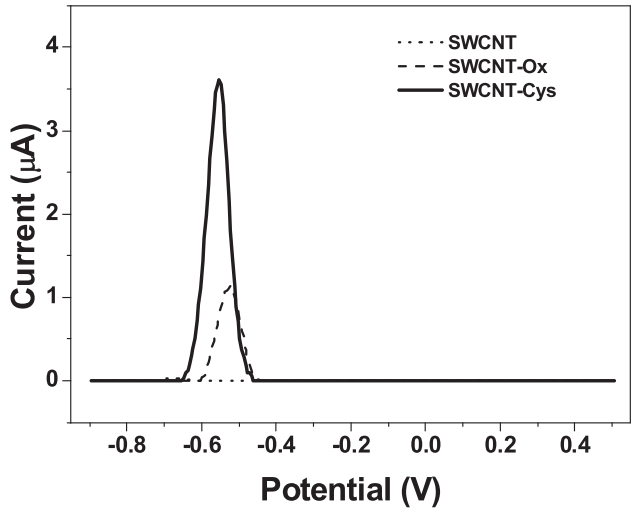

Fig. 3. LSAdSV recordings at SWCNT/GCE, SWCNT-Ox/GCE, SWCNT-Cys/GCE in 0.020 molL^{-1} ABS pH 5.00 containing 60 μg·L^{-1} Pb(II) Accumulation (pre-concentration) at OCP for 7 min, reduction time: 3 min, scan rate: 0.150 Vs^{-1}.

new oxygen groups, specifically carboxylic groups, which is detected at 1724 cm^{-1} [47]. Under these conditions, within the assayed range of pH values it is not possible to determine the isoelectric point. After the coupling of Cys-residues, SWCNT-Cys exhibit a slightly lower electrostatic charge compared to SWCNT-Ox demonstrating the efficient functionalization of SWCNT. These results are in accordance with those obtained by FTIR, where a consumption of carboxylic groups after Cys coupling reaction is evidenced by the increase in the band ratio between the one at 1724 cm^{-1} and the rest of carbonyl-based bands, appearing in the range of 1550–1750 cm^{-1}. New contributions between 1600 and 1624 cm^{-1} are observed in this region, which becomes much more populated after reaction, due to the presence of the amide bond, giving account of the efficient Cys-functionalization step [45].

In order to analyze the behavior of the proposed platform for the detection and quantification of lead, SWCNT/GCE, SWCNT-Ox/GCE and SWCNT-Cys/GCE were challenged with a 60 μgL^{-1} Pb(II) in 0.020 molL^{-1} acetate buffer solution pH 5.00 (ABS) (Scheme 1). As can be observed in Fig. 3, SWCNT/GCE platform is non-reactive for Pb(II) recognition due to either the nature or the low amount of available groups for Pb(II) affinity interaction. SWCNT-Ox/GCE and SWCNT-Cys/GCE allow Pb(II) detection because of the affinity of the oxygenated groups of both surfaces [48]. However, the affinity of Cys residues by Pb(II), makes possible a more selective and efficient accumulation of these metal ion [40], being the response with the platform SWCNT-Cys/GCE almost three times higher than the one for SWCNT-Ox/GCE ((3.6 ± 0.5) μA vs (1.3 ± 0.4) μA, respectively), demonstrating the advantages of the platform SWCNT-Cys/GCE.

3.2. Optimization of Pb(II) quantification and analytical performance of SWCNT-Cys/GCE

The experimental parameters for the detection of Pb(II) were critically evaluated to obtain the best compromise between sensitivity and reproducibility. The accumulation time (pre-concentration step) at OCP, the complex formation with thiol (SH) groups of Cys and the reduction time at −0.900 V before the stripping step were evaluated through the final stripping signal of Pb(II). For the optimization of the preconcentration step at OCP, times of 1.0, 3.0, 5.0, 7.0 and 10.0 min were investigated (results not shown). The maximum response for 60 μgL^{-1} Pb(II) solution was reached at 7.0 min, remaining almost constant for higher times. For the selection of the best reduction time at −0.900 V, times ranging from 1.0 to 5.0 min were assayed, being

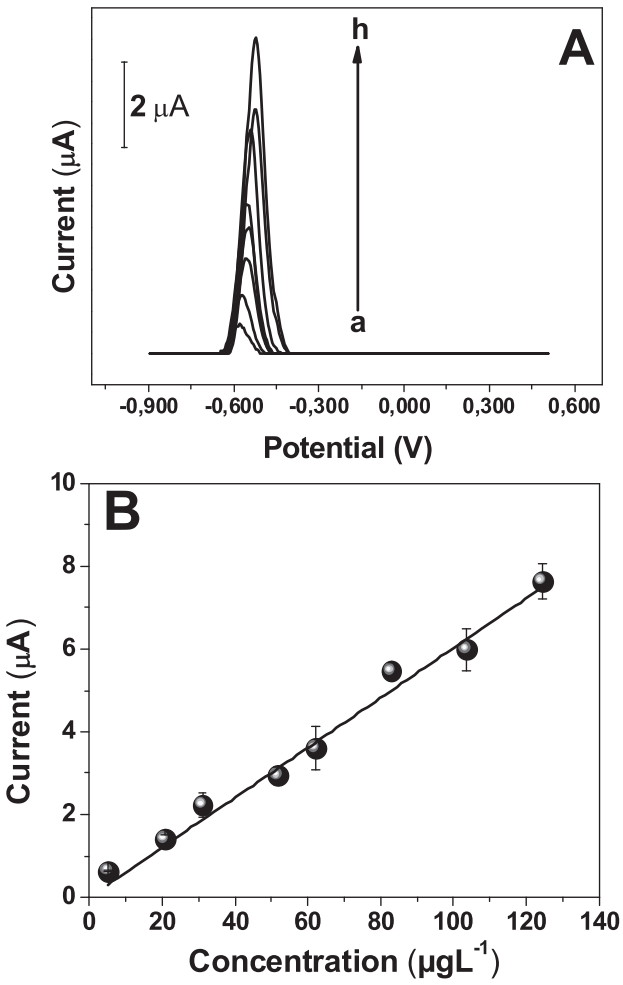

Fig. 4. A) LSAdSV at SWCNT-Cys/GCE with different concentrations, from 5 to 125 μg·L^{-1} Pb(II). B) LSAdSV calibration plot at SWCNT-Cys/GCE corresponding to the peak current in LSASV. Supportin electrolite: 0.020 molL^{-1} ABS pH 5.0 Deposition potential: OCP, deposition time: 7 min, reduction time: 3 min, scan rate: 0.150 Vs^{-1}.

3.0 min the one that allowed to obtain the best compromise between sensitivity and reproducibility. Therefore, for further experiments the selected conditions were 7.0 min preconcentration step at OCP, followed by 3.0 min at −0.900 V and the re-oxidation by a potential scan from –0.900 V to +0.800 V at a scan rate of 0.150 Vs^{-1}.

Fig. 4A. displays the current–potential profiles obtained for different concentrations of Pb(II) while the corresponding calibration plot is shown in Fig. 4B. The linear relationship between current and Pb(II) concentration ranges from 5 to 125 μg·L^{-1}. It is important to remark that this range comprises lower Pb(II) values than the maximum concentration of Pb(II) allowed by WHO in water for human consumption (10 μg·L^{-1}) [12]. The average sensitivity of biosensor was (0.061 ± 0.001) μA/μg·L^{-1}, with a correlation coefficient of 0.995. The detection limit, calculated as 3.3 × σ/S (where σ is the standard deviation of noise blank signal and S the sensitivity), was 0.69 μg·L^{-1}.

The biosensor ability for the specific detection of Pb(II) is a very important issue to evaluate. Considering that Hg(II) and Cd(II) are the most critical interferents due to the affinity of Cys by them, the selectivity of the proposed biosensor was evaluated in presence and absence of Hg(II) and Cd(II). Fig. 5. A. exhibits the current–potential profiles obtained for Pb(II) 60 μg·L^{-1} in absence and in presence of Hg (II) 400 μg·L^{-1} and Cd(II) 100 μg·L^{-1}. This figure shows the behavior and potential separation of Cd(II), Pb(II), and Hg(II) which appear at

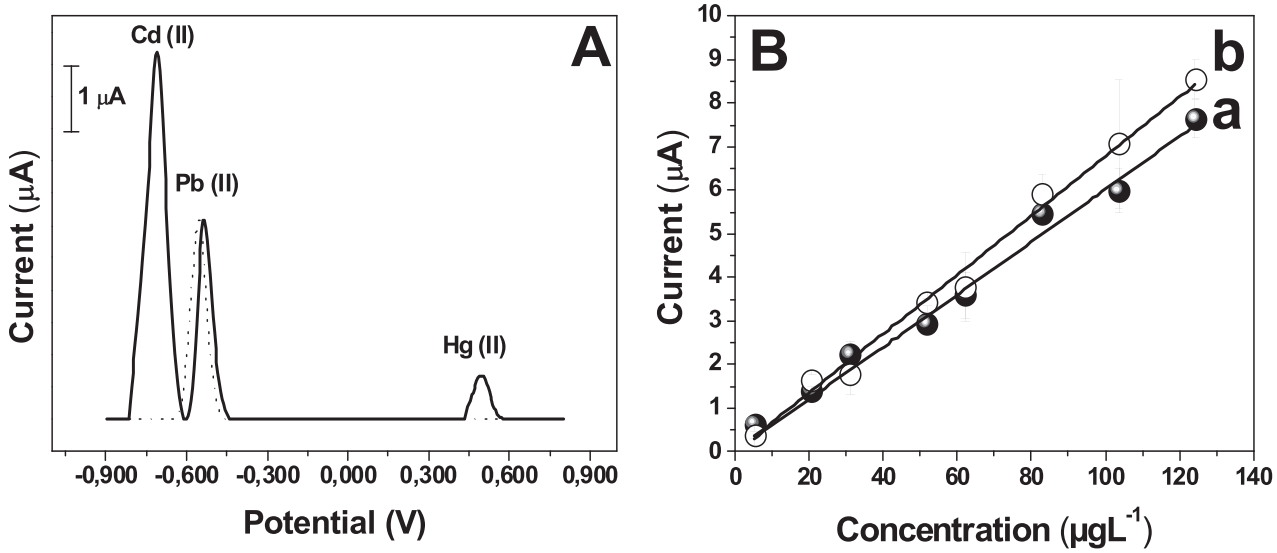

Fig. 5. A) LSAdSV recordings at SWCNT-Cys/GCE for 60 μg·L^{-1} Pb(II) (dashed line) and 60 μg·L^{-1} Pb(II) with 100 μg·L^{-1} Cd(II) and 400 μg·L^{-1}Hg(II) (solid line) B) Calibration plots at SWCNT-Cys/GCE in 0.020 molL^{-1} ABS pH 5.0 for 5 to 125 μg·L^{-1} Pb(II) in absense (a) and in presence of 100 μg·L-1 Cd(II) and 400 μg·L-1 Hg(II) (b). Deposition potential: OCP, deposition time: 7 min, reduction time: 3 min, scan rate: 0.150 Vs^{-1}. Results are presented as mean ± SD (error bar) of triplicate experiments.

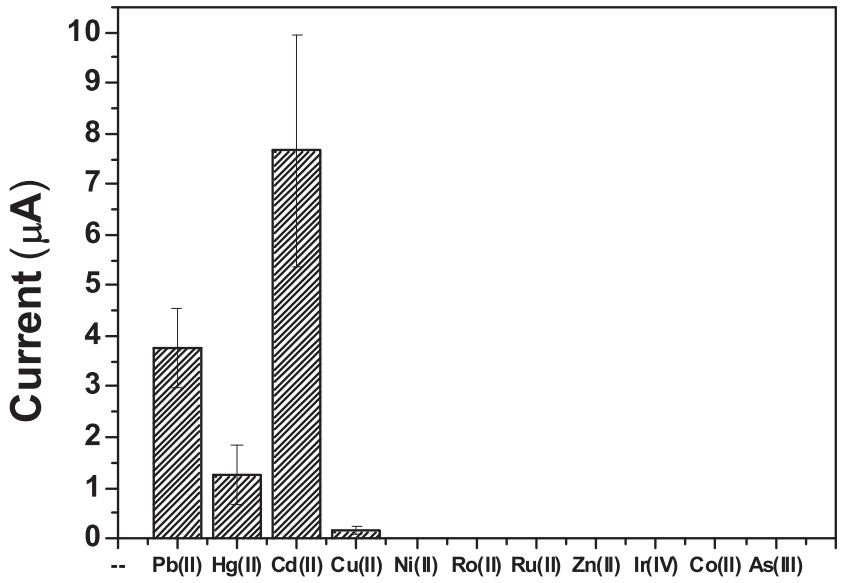

Fig. 6. Absolute current response from LAdSV recordings of SWCNT-Cys/GCE in 0.020 molL^{-1} ABS pH 5.0 for different species: 60 μg·L^{-1} Pb(II), 20 μg·L^{-1} Cu(II), 100 μg·L^{-1} Cd (II), Ni (II), Rh(II), Ru(II), Zn(II), Ir(IV), Co(II), As(III) and 400 μg·L^{-1} Hg(II). Deposition potential: OCP, deposition time: 7 min, reduction time: 3 min, scan rate: 0.150 Vs^{-1}. Results are presented as mean ± SD (error bar) of triplicate experiments.

around −0.700 V, −0.540 V and +0.500 V, respectively, revealing that the current peaks are separated enough avoiding the mutual interference and allowing Pb(II) selective detection. A similar experiment using the same concentrations of Pb(II), Cd(II) and Hg(II) was performed in order to compare the behavior of the different surfaces (SWCNT-Cys/GCE, SWCNT-Ox/GCE and SWCNT/GCE) in the presence of the three heavy metals. No response was observed for Pb (II) neither in the absence (as discussed in Fig. 3) nor in the presence of Cd(II) and Hg(II) (Fig. 3 SI). However, at SWCNT-Ox/GCE small oxidation signals are observed for Pb (II) and Cd(II), while for Hg(II) there is no response. It is important to mention that, at variance with SWCNT-Ox/GCE, at Cys-modified platform there are higher signals for the simultaneous oxidation of Pb(II) and Cd(II) and it is also possible to obtain a well-defined signal for Hg(II), clearly demonstrating the advantages of SWCNT-Cys/GCE (Fig. 3 SI)·The corresponding calibration plots for Pb (II) at SWCNT-Cys/GCE in absence and in presence of 100 μg·L^{-1} Cd(II) and 400 μg·L^{-1} Hg(II) are illustrated in Fig. 5. B. As can be observed, the sensitivities are (0.061 ± 0.001) μA/μg·L^{-1} (R^2 = 0.995) and (0.068 ± 0.006) μA/μg·L^{-1} (R^2 = 0.998) in the absence and presence of Cd(II) and Hg(II), respectively. This information is indicative that the performance of the sensor is not affected by the presence of these potential interferents. The biosensor was further challenged with 400 μg·L^{-1} of Hg(II), 100 μg·L^{-1}each Co(II), Zn(II), Ni(II), Cr(III), As (III), Ir(IV), Cd(II) and 20 μg·L^{-1} of Cu(II), in the presence of 60 μg·L^{-1} Pb(II). Fig. 6. displays the absolute measured currents (obtained from LAdSV recordings, data not shown) of Pb(II) and its potential interferents. It is important to remark that only Cd(II), Hg (II) and Cu(II), in addition to Pb(II) present oxidation signals. The oxidation signal of Cu (II) appears at around +0.030 V. Under these conditions, the biosensing platform efficiently discriminates Pb(II) from the assayed species demonstrating that it allows the highly selective detection of Pb(II).

Information about analytical parameters of different Pb(II)

Table 1
Analytical performance comparison of SWCNT-Cys/GCE with different reported platforms for Pb(II) detection.

Electrode	Method	Sensitivity	Detection limit	Detection range	Accumulation potential	Comments	Ref.
GO/MWCNTs/GCE	ASV	0.1914 μA ppm^{-1}	0.2 ppb	0.5–30 ppb	−1.4 V	Analyzed interferents: Zn^{2+}, Cd^{2+} and Cu^{2+} Real Sample: electroplating effluent samples Accumulation time: 180 seg.	[46]
Bi/CMWCNTs-β-CD-Nafion/GCE	SWASV	0.3345 μA ppm^{-1}	0.21 ppb	1.0–100 ppb	−1.2 V	Analyzed interferents: Cd^{2+}, Cu^{2+}, Na^{+}, As^{3+}, Cr^{2+}, K^{+}, Ca^{2+} and Zn^{2+} Real Sample: real soil samples Accumulation time: 140 seg.	[47]
L-cys/GR–CS/GCE	DPASV	0.745 μA ppm^{-1}	0.45 ppb	1.04–62.1 ppb	−1.1 V	Analyzed interferents: phenolics and inorganic salt ions Real Sample: Laoshan honey- wuxi rice Accumulation time: 120 seg.	[48]
Au-GN-Cys/GCE	SWASV	0.58 μA ppm^{-1}	0.050 ppb	0.5–40 ppb	−1.2 V	Analyzed interferents: Cd^{2+}, Co^{2+}, Fe^{3+}, Ni^{2+}, Cr^{3+}, Zn^{2+}, Cu^{2+}, In^{3+} and Sn^{2+} Real Sample: spring water from Yuelu Mountain. Accumulation time: 800 seg.	[49]
Au/CNFs/GCE	SWASV	2,36,803 μA μM	20 ppb	20 to 207 ppb	−1.8 V	Analyzed interferents: - Real Sample: - Accumulation time: 150 seg.	[50]
Bi/rGOCNT/AuE	SWASV	926 nA/ppbcm2	0.2 ppb	20 ppb to 200 ppb	−1.4 V	Analyzed interferents: K^{+}, Na^{+}, Ca^{2+}, Cl^{-}, NO^{3-}, Fe^{3+}, Cu^{2+} Real Sample: drinking water Accumulation time: 150 seg.	[51]
MnFe2O4@Cys/GCE	SWASV	35.3 mA/mM	0.0607 μM	0.2–1.1 μM	−1.5 V	Analyzed interferents: Zn(II), Ni(II), Co(II), Fe(III), Na(I), Cd(II), Cu(II) Real Sample: river water Accumulation time: 150 seg.	[52]
MWCNT-EBP-NA/GCE	SWASV	0.66562 μA/μg L^{-1}	0.08 μg L^{-1}	1.0 to 50.0 μg·L^{-1}	−1.4 V	Analyzed interferents: Cu^{2+}, Na^{+}, As^{3+}, Cr^{2+}, K^{+}, Ca^{2+}, Zn^{+2} and Cd^{+2} Real Sample: soil samples Accumulation time: 120 seg.	[53]
RGO-CS/PLL/GCE	DPASV	0.45 μA/μg L^{-1}	0.02 μg L^{-1}	0.05–2.0 μg L^{-1}	−1.2 V	Analyzed interferents: Zn(II), Mn(II), Ni(II), Fe(II), Fe(III), Co(II), Mg(II), Ba(II), Ca(II), Al(III), K(I), Ag(I), Na(I) Cd(II) and Cu(II) Real Sample: tap water Accumulation time: 180 seg.	[54]
SWCNT-Cys/GCE	LSAdSV	0.061 ± 0.001 μA/μg·L^{-1}	0.69 μg L^{-1}	5–125 μg L^{-1}	OCP	Analyzed interferents: Cu(II), Cd(II), Ni (II), Hg(II), Rh(II), Ru(II), Zn(II), Ir(IV),Co(II) and As(III) Real Sample: tap water and rain water Accumulation time: 180 seg.	This work

Graphene oxide (GO), multi-walled carbon nanotubes (MWCNTs), glassy carbon electrode (GCE), bismuth film (Bi), carboxylic acid functionalized multi-walled carbon nanotubes (CMWCNTs), β-cyclodextrin (β-CD), chitosan (CS), tiol (SH), L-cysteine (L-cys). Graphene reduced (GR), gold nanoparticle (Au), Graphene (GN), carbon nanofibers (CNFs), cysteine (Cys), single-walled carbon nanotubes (SWCNT), square wave anodic stripping voltammetry (SWASV), reduced graphene oxide carbon nanotubes (rGOCNT), gold electrode (AuE), multi-walled carbon nanotube-ion liquid (MWNT-IL), screen-printed carbon electrod (SPCE), L-cysteine functionalized mesoporous MnFe2O4 hybrid nanospheres (MnFe2O4@Cys), −emeraldine base polyaniline (EBP), Nafion (NA), reduced graphene oxide (RGO), poly-L-lysine films (PLL).

electrochemical sensors and biosensors reported in the last years are listed in Table 1. It is worthy to mention that the proposed biosensor in addition to the excellent performance, exhibits an outstanding operational property compared to the rest of the published electrochemical devices. All the sensors and biosensors reported in bibliography require of extremely high cathodic potentials, ranging from −1.10 V to −1.80 V for Pb(II) accumulation step [49–57], since all of them take advantage of the cation reduction for the subsequent stripping detection. In addition, the medium exchange step of the proposed sensing methodology, ensure the increase of the specificity in the presence of possible interferents (metals cations and other species). In addition, most of them display higher accumulation times, increasing the total time of the assay. Other interesting features of SWCNT-Cys/GCE are the comparable or smaller detection limits and similar or wider dynamic linear range than most of the sensing protocols already published (Table 1). In the present detection protocol, the biosensor is able to bind Pb(II) at OCP, without the need of elevated cathodic potentials, since the recognition event proceeded by affinity interactions which contributes to the high specificity of the assay. In summary, the biosensing platform based on SWCNT modified with Cys residues becomes an excellent and advantageous option for the highly sensitive, selective, easy and low-cost quantification of Pb(II) even in the presence of high concentrations of possible intereferents such as metals and other reducible species.

The practical application of the proposed electrochemical biosensor was evaluated from the point of view of its operational performance in recovery assays of Pb(II) in tap water samples taken from Cordoba city (Argentina) by triplicate. The obtained values are summarized in Table 2. The biosensor was validated using ICP-MS. For this assay, 0, 5.0 and 30.0 μg·L^{-1} Pb(II) were added to tap water showing excellent results for its determination, demonstrating an outstanding agreement with ICP-MS results. Further recovery assays were performed comparing tap and rain water with the addition of 60.0 μg·L^{-1} Pb(II) each by triplicate. The recovery was 98.3% (59 ± 7 μg·L^{-1}) from tap water and 100% (60 ± 5 μg·L^{-1}) from rain water, displaying a highly reproducible behavior of the proposed biosensor in both samples.

Table 2
Determination of Pb(II) on SWCNT-Cys/GCE in tap water and rain water samples. LSASV with a deposition potencial: OCP, deposition time: 7 min, reduction time: 3 min, scan rate: 0.150 Vs^{-1}.

Real sample	Pb(II) concentration added ($\mu g \cdot L^{-1}$)	Pb(II) concentration detected ($\mu g \cdot L^{-1}$)	Recovery (%)
Tap water	5.0	4.5	90.0
Tap water	60.0	58.5	97.6
Rain water	60.0	60.4	100.6

4. Conclusions

We have demonstrated the advantages of a novel electrochemical affinity sensing platform for Pb(II) quantification using GCE modified with an aqueous dispersion of SWCNT covalently functionalized with Cys moieties. The proposed sensor presents the great advantage that the accumulation of Pb(II) is based on the complex formation through the affinity interaction with Cys without the need of highly cathodic potentials. The affinity binding Cys-Pb(II) highly contributes to the enhancement of the selectivity of the biosensor. SWCNT-Cys/GCE proved to be a very suitable biodetection platform for the highly sensitive and selective Pb(II) quantification in the presence of elevated concentrations of other heavy metal species in water samples, showing an excellent correlation with ICP-MS. These outstanding analytical characteristics make SWCNT-Cys/GCE an interesting alternative for the evaluation of environmental damage.

Acknowledgements

The authors are grateful to CONICET (PIP 2015 Project N° 11220150100710CO), SECyT-UNC (PID Project 2016-2017 SIGEVA N° 30720150101013CB), ANPCyT (Projects : PICT 2013 N° 2817, PICT 2015 N° 0077) and MINCyT-Córdoba (PID Project N° 000018/2014), Spanish Ministry of Economy and Competitiveness (MINECO) project ENE2013-48816-C5-5-R, and the Government of Aragon and the European Social Fund under project grant DGA-FSE-T66 CNN for the financial support given to this work. M.L.R. and C.S.T. acknowledge doctoral fellowships from CONICET.

Appendix A. Supplementary data

Supplementary data to this article can be found online at https://doi.org/10.1016/j.microc.2018.05.007.

References

[1] X. Wang, J. Liu, Q. Tan, J. Ren, D. Liang, W. Fan, Development of multi-metal interaction model for Daphnia magna: significance of metallothionein in cellular redistribution, Ecotoxicol. Environ. Saf. 151 (2018) 42–48, http://dx.doi.org/10.1016/j.ecoenv.2017.12.040.
[2] E.S. Bernhardt, E.J. Rosi, M.O. Gessner, Synthetic chemicals as agents of global change, Front. Ecol. Environ. 15 (2017) 84–90, http://dx.doi.org/10.1002/fee.1450.
[3] C.N. Waters, J. Zalasiewicz, C. Summerhayes, A.D. Barnosky, C. Poirier, A. Gałuszka, A. Cearreta, M. Edgeworth, E.C. Ellis, M. Ellis, C. Jeandel, R. Leinfelder, J.R. McNeill, D.D.B. Richter, W. Steffen, J. Syvitski, D. Vidas, M. Wagreich, M. Williams, A. Zhisheng, J. Grinevald, E. Odada, N. Oreskes, A.P. Wolfe, The Anthropocene is functionally and stratigraphically distinct from the Holocene, Science (80-.) 351 (2016), http://dx.doi.org/10.1126/science.aad2622.
[4] I.A. Wright, M.M. Ryan, Impact of mining and industrial pollution on stream macroinvertebrates: importance of taxonomic resolution, water geochemistry and EPT indices for impact detection, Hydrobiologia 772 (2016) 103–115, http://dx.doi.org/10.1007/s10750-016-2644-7.
[5] X. Wu, S.J. Cobbina, G. Mao, H. Xu, Z. Zhang, L. Yang, A review of toxicity and mechanisms of individual and mixtures of heavy metals in the environment, Environ. Sci. Pollut. Res. 23 (2016) 8244–8259, http://dx.doi.org/10.1007/s11356-016-6333-x.
[6] F. Mancuso, I. Arato, C. Lilli, C. Bellucci, M. Bodo, M. Calvitti, M.C. Aglietti, M. dell'Omo, C. Nastruzzi, R. Calafiore, G. Luca, L. Marinucci, Acute effects of lead on porcine neonatal Sertoli cells in vitro, Toxicol. in Vitro 48 (2018) 45–52, http://dx.doi.org/10.1016/j.tiv.2017.12.013.
[7] M.B. Gumpu, S. Sethuraman, U.M. Krishnan, J.B.B. Rayappan, A review on detection of heavy metal ions in water - an electrochemical approach, Sensors Actuators B Chem. 213 (2015) 515–533, http://dx.doi.org/10.1016/j.snb.2015.02.122.
[8] Z. Xu, J. Wu, H. Li, Y. Chen, J. Xu, L. Xiong, J. Zhang, Characterizing heavy metals in combined sewer overflows and its influence on microbial diversity, Sci. Total Environ. 625 (2018) 1272–1282, http://dx.doi.org/10.1016/j.scitotenv.2017.12.338.
[9] T.A. Ayandiran, O.O. Fawole, S.O. Dahunsi, Water quality assessment of bitumen polluted Oluwa River, South-Western Nigeria, Water Resour. Ind. 19 (2018) 13–24, http://dx.doi.org/10.1016/j.wri.2017.12.002.
[10] S. Pan, L. Lin, F. Zeng, J. Zhang, G. Dong, B. Yang, Y. Jing, S. Chen, G. Zhang, Z. Yu, G. Sheng, H. Ma, Effects of lead, cadmium, arsenic, and mercury co-exposure on children's intelligence quotient in an industrialized area of southern China, Environ. Pollut. 235 (2018) 47–54, http://dx.doi.org/10.1016/j.envpol.2017.12.044.
[11] M. Jaishankar, T. Tseten, N. Anbalagan, B.B. Mathew, K.N. Beeregowda, Toxicity, mechanism and health effects of some heavy metals, Interdiscip. Toxicol. 7 (2014) 60–72, http://dx.doi.org/10.2478/intox-2014-0009.
[12] WHO, Lead in drinking-water, Guidel. Drink. Qual. 9 2003, http://dx.doi.org/10.1155/2013/959637.
[13] N.S. La Colla, C.E. Domini, J.E. Marcovecchio, S.E. Botté, Latest approaches on green chemistry preconcentration methods for trace metal determination in seawater - a review, J. Environ. Manag. 151 (2015) 44–55, http://dx.doi.org/10.1016/j.jenvman.2014.11.030.
[14] M.E. Genovese, G. Caputo, G. Nanni, C. Setti, M. Bustreo, G. Perotto, A. Athanassiou, D. Fragouli, Light responsive silk nanofibers: an optochemical platform for environmental applications, ACS Appl. Mater. Interfaces 9 (2017) 40707–40715, http://dx.doi.org/10.1021/acsami.7b13372.
[15] B.K. Bansod, T. Kumar, R. Thakur, S. Rana, I. Singh, A review on various electrochemical techniques for heavy metal ions detection with different sensing platforms, Biosens. Bioelectron. 94 (2017) 443–455, http://dx.doi.org/10.1016/j.bios.2017.03.031.
[16] S. Khan, A. Malik, Toxicity Evaluation of Textile Effluents and Role of Native Soil Bacterium in Biodegradation of a Textile Dye, (2017).
[17] J. Liu, H. Chen, L. Yao, Z. Wei, L. Lou, Y. Shan, S.D. Endalkachew, N. Mallikarjuna, B. Hu, X. Zhou, The spatial distribution of pollutants in pipe-scale of large-diameter pipelines in a drinking water distribution system, J. Hazard. Mater. 317 (2016) 27–35, http://dx.doi.org/10.1016/j.jhazmat.2016.05.048.
[18] M. Del Rio, J. Alvarez, T. Mayorga, S. Dominguez, C. Sobin, A comparison of arsenic exposure in young children and home water arsenic in two rural West Texas communities, BMC Public Health 17 (2017) 1–13, http://dx.doi.org/10.1186/s12889-017-4808-4.
[19] A. Ashraf, E. Saion, E. Gharibshahi, H.M. Kamari, C.K. Yap, M.S. Hamzah, M.S. Elias, Distribution of trace elements in core marine sediments of coastal East Malaysia by instrumental neutron activation analysis, Appl. Radiat. Isot. 122 (2018) 96–105, http://dx.doi.org/10.1016/j.apradiso.2017.01.006.
[20] L. Yuanyuan, L. Xinqiang, C. Niyungeko, Z. Junjie, T. Guangming, A review of the identification and detection of heavy metal ions in the environment by voltammetry, Talanta 178 (2018) 324–338, http://dx.doi.org/10.1016/j.talanta.2017.08.033.
[21] J. Mehta, S.K. Bhardwaj, N. Bhardwaj, A.K. Paul, P. Kumar, K.H. Kim, A. Deep, Progress in the biosensing techniques for trace-level heavy metals, Biotechnol. Adv. 34 (2016) 47–60, http://dx.doi.org/10.1016/j.biotechadv.2015.12.001.
[22] P. Kumar, K.-H. Kim, V. Bansal, T. Lazarides, N. Kumar, Progress in the sensing techniques for heavy metal ions using nanomaterials, J. Ind. Eng. Chem. 54 (2017) 30–43, http://dx.doi.org/10.1016/j.jiec.2017.06.010.
[23] G.M.S. Alves, L.S. Rocha, H.M.V.M. Soares, Multi-element determination of metals and metalloids in waters and wastewaters, at trace concentration level, using electroanalytical stripping methods with environmentally friendly mercury free-electrodes: a review, Talanta 175 (2017) 53–68, http://dx.doi.org/10.1016/j.talanta.2017.06.077.
[24] L. Cui, J. Wu, H. Ju, Electrochemical sensing of heavy metal ions with inorganic, organic and bio-materials, Biosens. Bioelectron. 63 (2015) 276–286, http://dx.doi.org/10.1016/j.bios.2014.07.052.
[25] G. Maduraiveeran, M. Sasidharan, V. Ganesan, Electrochemical sensor and biosensor platforms based on advanced nanomaterials for biological and biomedical applications, Biosens. Bioelectron. 103 (2018) 113–129, http://dx.doi.org/10.1016/j.bios.2017.12.031.
[26] H. Ju, Functional nanomaterials and nanoprobes for amplified biosensing, Appl. Mater. Today 10 (2018) 51–71, http://dx.doi.org/10.1016/j.apmt.2017.11.001.
[27] G.A. Rivas, M.C. Rodríguez, M.D. Rubianes, F.A. Gutierrez, M. Eguílaz, P.R. Dalmasso, E.N. Primo, C. Tettamanti, M.L. Ramírez, A. Montemerlo, P. Gallay, C. Parrado, Carbon nanotubes-based electrochemical (bio)sensors for biomarkers, Appl. Mater. Today 9 (2017) 566–588, http://dx.doi.org/10.1016/j.apmt.2017.10.005.
[28] J. Huang, X. Su, Z. Li, Metal ion detection using functional nucleic acids and nanomaterials, Biosens. Bioelectron. 96 (2017) 127–139, http://dx.doi.org/10.1016/j.bios.2017.04.032.
[29] Y. Wang, S. Hu, Applications of carbon nanotubes and graphene for electrochemical sensing of environmental pollutants, J. Nanosci. Nanotechnol. 16 (2016) 7852–7872, http://dx.doi.org/10.1166/jnn.2016.12762.
[30] J. Wang, M. Musameh, Y. Lin, Solubilization of carbon nanotubes by Nafion toward the preparation of amperometric biosensors, J. Am. Chem. Soc. 125 (2003) 2408–2409, http://dx.doi.org/10.1021/ja028951v.
[31] M.D. Rubianes, G.A. Rivas, Dispersion of multi-wall carbon nanotubes in polyethylenimine: a new alternative for preparing electrochemical sensors,

Electrochem. Commun. 9 (2007) 480–484, http://dx.doi.org/10.1016/j.elecom.2006.08.057.
[32] Y. Jalit, M.C. Rodríguez, M.D. Rubianes, S. Bollo, G.A. Rivas, Glassy carbon electrodes modified with multiwall carbon nanotubes dispersed in polylysine, Electroanalysis 20 (2008) 1623–1631, http://dx.doi.org/10.1002/elan.200804259.
[33] S. Gupta, C.N. Murthy, C.R. Prabha, Recent advances in carbon nanotube based electrochemical biosensors, Int. J. Biol. Macromol. 108 (2018) 687–703, http://dx.doi.org/10.1016/j.ijbiomac.2017.12.038.
[34] C. Gao, Z. Guo, J.-H. Liu, X.-J. Huang, The new age of carbon nanotubes: an updated review of functionalized carbon nanotubes in electrochemical sensors, Nano 4 (2012) 1948, http://dx.doi.org/10.1039/c2nr11757f.
[35] S.W. Kim, T. Kim, Y.S. Kim, H.S. Choi, H.J. Lim, S.J. Yang, C.R. Park, Surface modifications for the effective dispersion of carbon nanotubes in solvents and polymers, Carbon N. Y. 50 (2012) 3–33, http://dx.doi.org/10.1016/j.carbon.2011.08.011.
[36] E.N. Primo, F.A. Gutierrez, G.L. Luque, P.R. Dalmasso, A. Gasnier, Y. Jalit, M. Moreno, M.V. Bracamonte, M.E. Rubio, M.L. Pedano, M.C. Rodríguez, N.F. Ferreyra, M.D. Rubianes, S. Bollo, G.A. Rivas, Comparative study of the electrochemical behavior and analytical applications of (bio)sensing platforms based on the use of multi-walled carbon nanotubes dispersed in different polymers, Anal. Chim. Acta 805 (2013) 19–35, http://dx.doi.org/10.1016/j.aca.2013.10.039.
[37] D. Baskaran, J.W. Mays, M.S. Bratcher, V. Uni, B. Hall, V. Knox, R.V. December, V. Re, M. Recei, V. March, Noncovalent and Nonspecific Molecular Interactions of Polymers with Multiwalled Carbon Nanotubes, 80 (2005), pp. 3389–3397.
[38] M. Eguílaz, C.J. Venegas, A. Gutiérrez, G.A. Rivas, S. Bollo, Carbon nanotubes noncovalently functionalized with cytochrome c: a new bioanalytical platform for building bienzymatic biosensors, Microchem. J. 128 (2016) 161–165, http://dx.doi.org/10.1016/j.microc.2016.04.018.
[39] M. Eguílaz, A. Gutiérrez, F. Gutierrez, J.M. González-Domínguez, A. Ansón-Casaos, J. Hernández-Ferrer, N.F. Ferreyra, M.T. Martínez, G. Rivas, Covalent functionalization of single-walled carbon nanotubes with polytyrosine: characterization and analytical applications for the sensitive quantification of polyphenols, Anal. Chim. Acta 909 (2016) 51–59, http://dx.doi.org/10.1016/j.aca.2015.12.031.
[40] N.C. Li, R.A. Manning, Some metal complexes of sulfur-containing amino acids, J. Am. Chem. Soc. 77 (1955) 5225–5228, http://dx.doi.org/10.1021/ja01625a006.
[41] B.G. Shah, Chelating agents and bioavailability of minerals, Nutr. Res. 1 (1982) 617–622.
[42] A. Aliberti, P. Vaiano, A. Caporale, M. Consales, M. Ruvo, A. Cusano, Fluorescent chemosensors for hg 2+ detection in aqueous environment, Sensors Actuators B Chem. 247 (2017) 727–735, http://dx.doi.org/10.1016/j.snb.2017.03.026.
[43] C. Gilsanz, R. Gusmão, E. Chekmeneva, N. Serrano, J.M. Díaz-Cruz, C. Ariño, M. Esteban, Electroanalysis of the binding and adsorption of Hg2+ with seleno aminoacids by differential pulse and elimination voltammetry at the au-disk electrode, Electrochim. Acta 56 (2011) 5988–5992, http://dx.doi.org/10.1016/j.electacta.2011.04.102.
[44] P.R. Dalmasso, M.L. Pedano, G.A. Rivas, Electrochemical determination of cu(II) using a glassy carbon electrode modified with multiwall carbon nanotubes dispersed in polyhistidine, Electroanalysis 27 (2015) 2164–2170, http://dx.doi.org/10.1002/elan.201500116.
[45] F.A. Gutierrez, J.M. Gonzalez-Dominguez, A. Ansón-Casaos, J. Hernández-Ferrer, M.D. Rubianes, M.T. Martínez, G. Rivas, Single-walled carbon nanotubes covalently functionalized with cysteine: a new alternative for the highly sensitive and selective Cd(II) quantification, Sensors Actuators B Chem. 249 (2017) 506–514, http://dx.doi.org/10.1016/j.snb.2017.04.026.
[46] Y.M. Go, J.D. Chandler, D.P. Jones, The cysteine proteome, Free Radic. Biol. Med. 84 (2015) 227–245, http://dx.doi.org/10.1016/j.freeradbiomed.2015.03.022.
[47] J. Coates, R.A.M. Ed, J. Coates, Interpretation of infrared spectra, a practical approach interpretation of infrared spectra, a practical approach, Encycl. Anal. Chem. (2000) 10815–10837, http://dx.doi.org/10.1002/9780470027318.
[48] A. Ihsanullah, A.M. Abbas, T. Al-Amer, M.J. Laoui, M.S. Al-Marri, M. Nasser, M.A. Atieh Khraisheh, Heavy metal removal from aqueous solution by advanced carbon nanotubes: critical review of adsorption applications, Sep. Purif. Technol. 157 (2016) 141–161, http://dx.doi.org/10.1016/j.seppur.2015.11.039.
[49] H. Huang, T. Chen, X. Liu, H. Ma, Ultrasensitive and simultaneous detection of heavy metal ions based on three-dimensional graphene-carbon nanotubes hybrid electrode materials, Anal. Chim. Acta 852 (2014) 45–54, http://dx.doi.org/10.1016/j.aca.2014.09.010.
[50] G. Zhao, H. Wang, G. Liu, Z. Wang, Simultaneous determination of Cd(II) and Pb(II) based on bismuth film/carboxylic acid functionalized multi-walled carbon nanotubes-β-cyclodextrin-nafion nanocomposite modified electrode, Int. J. Electrochem. Sci. 11 (2016) 8109–8122, http://dx.doi.org/10.20964/2016.10.07.
[51] W. Zhou, C. Li, C. Sun, X. Yang, Simultaneously determination of trace Cd2+ and Pb2+ based on l-cysteine/graphene modified glassy carbon electrode, Food Chem. 192 (2016) 351–357, http://dx.doi.org/10.1016/j.foodchem.2015.07.042.
[52] L. Zhu, L. Xu, B. Huang, N. Jia, L. Tan, S. Yao, Simultaneous determination of Cd(II) and Pb(II) using square wave anodic stripping voltammetry at a gold nanoparticle-graphene-cysteine composite modified bismuth film electrode, Electrochim. Acta 115 (2014) 471–477, http://dx.doi.org/10.1016/j.electacta.2013.10.209.
[53] B. Zhang, J. Chen, H. Zhu, T. Yang, M. Zou, M. Zhang, M. Du, Facile and green fabrication of size-controlled AuNPs/CNFs hybrids for the highly sensitive simultaneous detection of heavy metal ions, Electrochim. Acta 196 (2016) 422–430, http://dx.doi.org/10.1016/j.electacta.2016.02.163.
[54] X. Xuan, J.Y. Park, A miniaturized and flexible cadmium and lead ion detection sensor based on micro-patterned reduced graphene oxide/carbon nanotube/bismuth composite electrodes, Sensors Actuators B Chem. 255 (2018) 1220–1227, http://dx.doi.org/10.1016/j.snb.2017.08.046.
[55] S.-F. Zhou, J.-J. Wang, L. Gan, X.-J. Han, H.-L. Fan, L.-Y. Mei, J. Huang, Y.-Q. Liu, Individual and simultaneous electrochemical detection toward heavy metal ions based on L-cysteine modified mesoporous MnFe 2 O 4 nanocrystal clusters, J. Alloys Compd. 721 (2017) 492–500, http://dx.doi.org/10.1016/j.jallcom.2017.05.321.
[56] G. Zhao, Y. Yin, H. Wang, G. Liu, Z. Wang, Sensitive stripping voltammetric determination of cd(II) and Pb(II) by a bi/multi-walled carbon nanotube-emeraldine base polyaniline-Nafion composite modified glassy carbon electrode, Electrochim. Acta 220 (2016) 267–275, http://dx.doi.org/10.1016/j.electacta.2016.10.059.
[57] Z. Guo, D. di Li, X. ke Luo, Y. hui Li, Q.N. Zhao, M. meng Li, Y. ting Zhao, T. shuai Sun, C. Ma, Simultaneous determination of trace Cd(II), Pb(II) and cu(II) by differential pulse anodic stripping voltammetry using a reduced graphene oxide-chitosan/poly-L-lysine nanocomposite modified glassy carbon electrode, J. Colloid Interface Sci. 490 (2017) 11–22, http://dx.doi.org/10.1016/j.jcis.2016.11.006.